Charged B decay and ditau anomalies from two-Higgs doublet models

Srobona Basak

Department of Physics
McGill University, Montréal

November, 2024

A thesis submitted to McGill University in partial fulfillment of the requirements of the degree of

Master of Science

Table of Contents

Abstract

There has been continued observation of an excess in the τ final states compared to the e, μ states in $B \to Dl\nu$ and $B \to D^* l\nu$ charged decays that is larger than expected from Standard Model computations. This thesis explores the viability of resolving the anomaly through a mediating light charged Higgs boson, H^+ from a general type III two-Higgs doublet model (2HDM) with a large coupling between the τ and the charged Higgs. In previous work [1], it was shown that this could be realised by a charged Higgs of mass $\sim$ 100 [GeV]. This motivated a combined analysis of the B-decay anomaly with the ditau as well as diphoton excesses observed by CMS suggesting a new Higgs of mass $\sim$ 95 [GeV]. The thesis starts by using the experimental results for R_D and R_{D*} as well as from the ditau excess to to constrain the parameter space of the new Yukawa couplings of the 2HDM. We also find that the cross-section for an SM-like Higgs boson to mediate diphoton final states from proton-proton collisions computed using our model is too weak to describe observations made by CMS. Finally, we compute the cross-section of the process $pp \to H \to \tau\tau^-$, where H is the hypothesized lighter SM-like Higgs boson, and plot it as a function of its mass and coupling with the top quark. We also show that the charged Higgs production predicted by the model is consistent with bounds from the cross-section of $\tau\tau$ final states resulting from proton-proton collisions.

Abrégé

Il y a eu une observation continue d'un excès dans les états finaux τ par rapport aux états e, μ dans les désintégrations chargées $B \to Dl\nu$ et $B \to D^* l\nu$ qui est plus grand que prévu par les calculs du Modèle Standard. Cette thèse explore la viabilité de la résolution de l'anomalie par un boson de Higgs chargé léger médiateur, H^+, à partir d'un modèle général de doublet de deux Higgs de type III (2HDM) avec un couplage important entre le τ et le Higgs chargé. Dans des travaux antérieurs [1], il a été montré que cela pouvait être réalisé par un Higgs chargé de masse ~ 100 [GeV]. Ceci a motivé une analyse combinée de l'anomalie de désintégration B avec le ditau ainsi que des excès de diphotons observés par CMS suggérant un nouveau Higgs de masse ~ 95 [GeV]. La thèse commence par utiliser les résultats expérimentaux pour R_D et R_{D*} ainsi que l'excès de ditau pour contraindre l'espace des paramètres des nouveaux couplages de Yukawa du 2HDM. Nous constatons également que la section efficace d'un boson de Higgs de type SM pour la médiation d'états finaux diphotoniques dans des collisions proton-proton calculée à l'aide de notre modèle est trop faible pour décrire les observations faites par CMS. Enfin, nous calculons la section efficace du processus $pp \to H \to \tau\tau^-$, où H est le boson de Higgs de type SM supposé plus léger, et nous la représentons en fonction de sa masse et de son couplage avec le quark supérieur. Nous montrons également que la production de Higgs chargés prédite par le modèle est cohérente avec les limites de la section efficace des états finaux $\tau\tau$ résultant des collisions proton-proton.

Acknowledgements

Firstly, I would like to express my sincerest gratitude to my supervisor, Prof. James Cline, for his support and guidance. His expertise and insight have been invaluable to me throughout working on this project. I am truly grateful to him for giving me the opportunity to pursue my long-term goal of doing research in particle theory and for helping me navigate through the academic challenges I faced, especially starting out as someone new to the field.

I am also deeply thankful to Prof. Robert Brandenberger for his mentorship throughout my time at McGill. His patience and attentiveness in explaining complex concepts have shaped my understanding of quantum field theory and been crucial in my academic development.

I would also like to thank my parents, Sanghita Sen and Syamal Kumar Basak, and my sister, Srutokirti Basak, for their constant support and encouragement.

Finally, I am incredibly grateful to all my friends in the Physics department with special thanks to Nirmalya Brahma, Erny Au Yang, Caitlyn Dewar, Dr. Saniya Heeba, Christian Capanelli, and Magnus L'Argent for the illuminating discussions, motivation, and unwavering support.

List of Figures

Introduction

Recent experimental analyses by the LHCb [2], BaBar [3], and Belle [4] collaborations show robust evidence for lepton flavor universality violation (LFUV) in charged $B \to D/D^* l\nu$ decays. This is measured by observing the ratio of decay rates involving τ lepton final states and those with e or μ final states in each process, denoted by R_D and R_{D^*} respectively. It can be seen from Fig.1 [5] that according to the experimental measurements, these ratios are about 10-15% larger than that predicted from the SM, with a significance of around 3σ. A possible explanation of these anomalies is that these new contributions come from the exchange of a light charged Higgs boson H^+, as proposed in two-Higgs doublet models (2HDMs) [1, 6]. However, these models face heavy constraints from the lifetime of the B_c meson due to $B_c \to \tau\nu$ decays as well as monojet production of $X\tau\nu$ in proton-proton collisions [7]. On the other hand, potential exceptions to these constraints have been considered in the literature [8].

CMS and more recently, ATLAS have observed an excess of diphoton events consistent with a neutral Higgs boson near 95 GeV [9, 10, 11]. In addition to this, a possible ditau excess around 0.1 TeV was discovered by CMS [12]. These anomalies could potentially be explained as being mediated by an additional lighter SM-like Higgs boson, H also proposed in 2HDMs. This possibility along with the prediction from [1] of light Higgs states with masses near 100 GeV led us to perform a combined analysis of all anomalies to evaluate their potential to support the 2HDM framework.

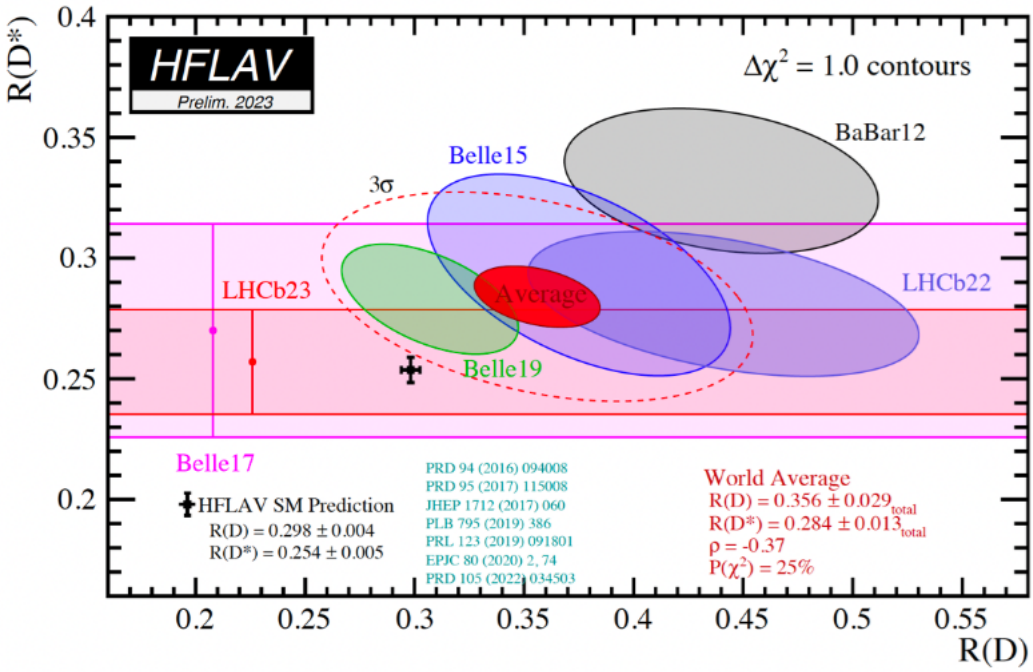

Figure 1: Compilation of the status of experimental results on the LFUV ratios R_D and R_{D^*}, represented by the coloured bands and ellipses in the plot, and their SM predictions, denoted by the black crosses, by the Heavy Flavour Averaging Group (HFLAV) [5]. The dotted red ellipse is the 3σ countour of the global average of the experimental results.

The thesis is organised as follows. The first chapter provides a description of the model and is mainly based on [13], [14], and [1]. The second chapter discusses experimental constraints on the model and addresses possible oppositions to it. Finally, the third chapter shows the results we obtained about the viability of the model in describing the experimental anomalies mentioned above according to our analysis.

Chapter 1

The Two-Higgs Doublet Model

1.1 Motivation

The Standard Model (SM) consists of only one Higgs doublet but there is no reason in general why this should be the case. On the contrary, there are several motivations to postulate the existence of a 'Higgs sector'. The 2HDM is one such theory where this is done by adding a second Higgs doublet to the existing theory. Some shortcomings of the SM that have the possibility to be resolved by this model are summarised below.

The first shortcoming involves axion models. It was shown by Peccei and Quinn [15] that a potential CP-violating term in the QCD Lagrangian can be eliminated if the Lagrangian has a global $U(1)$ symmetry. However, this symmetry can only be implemented if there are two Higgs doublets in the theory [14]. Another drawback of the SM is its inability to generate a large enough baryon asymmetry of the Universe. Two-Higgs doublet models can address this issue due to their flexible scalar mass spectrum and since they contain extra possible sources of CP violation [16].

Other motivations for the 2HDM is that it provides the necessary Higgs structure for supersymmetric models. Additionally, it is an extension to the SM that adds the fewest new

parameters to the theory while being consistent with constraints such as $\varrho = 1$. At tree level, the parameter ϱ is defined by [14]

$$\varrho = \frac{\sum_{i=1}^{n} \left[I_i(I_i+1) - \frac{1}{4}Y_i^2 \right] v_i}{\sum_{i=1}^{n} \frac{1}{2} Y_i^2 v_i}, \tag{1.1}$$

where I_i are the weak isospin, Y_i the weak hypercharge, v_i the VEVs of the neutral components in a $SU(2) \times U(1)$ gauge theory with n scalar multiplets ϕ_i. According to experimental data [17], $\varrho = 1.00058$. From the equation above, $\varrho = 1$ if $I(I+1) = \frac{3}{4}Y^2$, which is the case for $SU(2)$ doublets with $Y = \pm 1$. Other configurations such as scalars with VEVs in larger $SU(2)$ multiplets and scalars with small or null VEVs also give $\varrho = 1$, however these are often a lot more complicated than just adding a doublet or singlet.

A potential complication of 2HDMS is the presence of tree-level flavour changing neutral currents (FCNC), which are highly constrained. In a general 2HDM, the Yukawa coupling terms,

$$\mathcal{L}_Y = \bar{\psi}_i \hat{y}_{ij} \psi_j \phi_1 + \bar{\psi}_i \hat{\rho}_{ij} \psi_j \phi_2, \tag{1.2}$$

where i, j are the flavour indices, lead to the mass matrix

$$M = \frac{v_1}{\sqrt{2}} \hat{y} + \frac{v_2}{\sqrt{2}} \hat{\rho}. \tag{1.3}$$

Since there is only one Higgs doublet in the SM, therefore diagonalising M means that $\hat{y}$ is also diagonalised, which ensures that there are no tree-level FCNCs. However, this is not necessarily the case in 2HDMs, since in general, $\hat{y}$ and $\hat{\rho}$ need not be simultaneously diagonalisable, giving rise to flavour mixing. However, this can be resolved by introducing symmetries into the Lagrangian. For instance, if all the fermions with the same quantum numbers, i.e. the fermions that are allowed to mix with each other, couple to the same Higgs doublet, then we can avoid FCNCs. This can be enforced by introducing a $\mathcal{Z}_2$ symmetry,

$\phi_1 \to -\phi_1$. This results in all the fermions coupling to only ϕ_2. This is known as the Type I 2HDM. Alternatively, by imposing a $d_R^i \to -d_R^i$ in addition to $\phi_1 \to -\phi_1$, one obtains the type II 2HDM, where the $Q = 2/3$ right-handed (RH) quarks couple to ϕ_2 and the $Q = -1/3$ RH quarks couple to ϕ_1 [14]. A third more general type of 2HDMs is the type III 2HDM, where FCNCs exist at tree level and can be suppressed for instance by introducing a specific ansatz for the Yukawa couplings. This is the type of 2HDM that this thesis considers and the ansatz introduced to suppress the FCNCs in this case will be shown in Chapter 3.

1.2 The Scalar Potential

We shall consider the most general form of the 2HDM, also known as the Type III 2HDM. In this model, a minimal extension in the Higgs sector in the SM is made by introducing a complex $SU(2)_L$ doublet scalar field in addition to the SM one. Let these be ϕ_1 and ϕ_2. Then, the most general renormalisable scalar potential is given by

$$\begin{aligned} V = {} & m_{11}^2 \phi_1^\dagger \phi_1 + m_{22}^2 \phi_2^\dagger \phi_2 - (\tilde{m}_{12}^2 \phi_1^\dagger \phi_2 + \text{h.c.}) \\ & + \frac{1}{2}\Lambda_1 (\phi_1^\dagger \phi_1)^2 + \frac{1}{2}\Lambda_2 (\phi_2^\dagger \phi_2)^2 + \Lambda_3 (\phi_1^\dagger \phi_1)(\phi_2^\dagger \phi_2) + \Lambda_4 (\phi_1^\dagger \phi_2)(\phi_2^\dagger \phi_1) \\ & + \left[\frac{1}{2}\Lambda_5 (\phi_1^\dagger \phi_2)^2 + \Lambda_6 (\phi_1^\dagger \phi_1)(\phi_1^\dagger \phi_2) + \Lambda_7 (\phi_2^\dagger \phi_2)(\phi_1^\dagger \phi_2) + \text{h.c.} \right], \end{aligned} \tag{1.4}$$

where m_{11}^2, m_{22}^2, and $\Lambda_{1,2,3,4}$ are real parameters, and m_{12}^2 and $\Lambda_{5,6,7}$ are in general complex. Hence, at first glance there appears to be fourteen free parameters in total. However, we shall see later that the freedom to redefine fields implies that of these fourteen parameters, only eleven are physical.

1.3 The Higgs basis

It has been shown that the 2HDM admits only three types of vacua besides the case where $\langle\phi_1\rangle = \langle\phi_2\rangle = 0$, i.e. there are three types of configurations of the fields besides the trivial case that minimise the potential shown above [14]. The simplest of these is the SM-equivalent one given by

$$\langle\phi_1\rangle_0 = \begin{pmatrix} 0 \\ \frac{v_1}{\sqrt{2}} \end{pmatrix}, \qquad \langle\phi_2\rangle_0 = e^{i\delta} \begin{pmatrix} 0 \\ \frac{v_2}{\sqrt{2}} \end{pmatrix},$$

where v_1 and v_2 are real and $v = \sqrt{v_1^2 + v_2^2} = 246$ GeV. The other two configurations are CP-breaking vacua and charge-breaking vacua which will not be discussed here. At this point, it is convenient to transform to a basis where the VEV is completely in the first field. This is known as the Higgs basis and we can go to this basis using

$$H_i = \sum_{j=1}^{2} U_{ij}\phi_j, \tag{1.5}$$

where

$$U = \frac{e^{-i\delta/2}}{v} \begin{pmatrix} v_1 e^{i\delta/2} & v_2 e^{-i\delta/2} \\ -v_2 e^{i\delta/2} & v_1 e^{-i\delta/2} \end{pmatrix}, \tag{1.6}$$

is unitary. The parameter $\tan\beta = v_1/v_2$ is also defined. It should also be noted that it is possible to also introduce a relative phase between the two doublets at this point, implying the existence of an infinite number of Higgs bases. Now, we can expand the fields as follows:

$$H_1 = \tfrac{1}{\sqrt{2}} \begin{pmatrix} \sqrt{2}G^+ \\ v + h + iG^0 \end{pmatrix}, \qquad H_2 = \tfrac{1}{\sqrt{2}} \begin{pmatrix} \sqrt{2}H^+ \\ H + iA \end{pmatrix},$$

where $G^\pm$ are complex fields and h, H, G^0, and A are real fields. G^+ and G^0 are the massless Goldstone bosons produced as a result of spontaneous electroweak symmetry breaking that give rise to the longitudinal elements of the W^+ and Z^0 bosons. This leaves us with five

physical Higgs bosons, a pair of charged Higgs bosons, $H^{\pm}$, a neutral CP-odd Higgs, A, and two neutral CP-even Higgs, h and H.

This basis transformation also leads to the couplings in the scalar potential also being rotated such that the coefficients in the Higgs basis can now be expressed in terms of the parameters from the generic basis, in the process, eliminating redundant parameters. The freedom to introduce a relative phase between the two Higgs doublets implies that the couplings in the scalar potential are observable up to the overall phase of the complex parameters. This leaves us with only eleven physical parameters. The new potential is given by

$$\begin{aligned} V = \lambda \left(H_1^\dagger H_1 - \frac{v^2}{2} \right)^2 + m_2^2 (H_2^\dagger H_2) + m_{12}^2 (H_1^\dagger H_2 + H_2^\dagger H_1) + \lambda_1 (H_1^\dagger H_1)(H_2^\dagger H_2) \\ + \lambda_2 (H_1^\dagger H_2)(H_2^\dagger H_1) + 2\lambda_3 (H_1^\dagger H_2)^2 + \lambda_4 [(H_1^\dagger H_2)(H_2^\dagger H_2) + (H_2^\dagger H_1)(H_2^\dagger H_2)] \\ + \lambda_5 [(H_2^\dagger H_1)(H_1^\dagger H_1) + (H_1^\dagger H_2)(H_1^\dagger H_1)] + \lambda_6 (H_2^\dagger H_2)^2, \end{aligned} \tag{1.7}$$

where λ_i, m_2, and m_{12} are real parameters and $m_{12}^2 + \lambda_5^* v^2 = 0$. To simplify things, it is also assumed that V is CP-conserving so that there is no mixing between the scalars and pseudoscalar. The masses of the physical Higgs bosons are then given by

$$m_h^2 = 2\lambda v^2 \tag{1.8}$$

$$m_H^2 = m_2^2 + \frac{1}{2}(\lambda_1 + \lambda_2 + 2\lambda_3) v^2 \tag{1.9}$$

$$m_A^2 = m_H^2 - 2\lambda_3 v^2 \tag{1.10}$$

$$m_\pm^2 = m_2^2 + \frac{1}{2}\lambda_1 v^2. \tag{1.11}$$

1.4 The Yukawa Lagrangian

The Yukawa coupling part of the Lagrangian is

$$\mathcal{L}_Y = \hat{y}_u^{ij}\bar{Q}_L^i\tilde{H}_1 u_R^j + \bar{y}_d^{ij}\bar{Q}_L^i H_1 d_R^j + \bar{y}_e^{ij}\bar{L}_L^i H_1 e_R^j + \hat{\rho}_u^{ij}\bar{Q}_L^i\tilde{H}_2 u_R^j + \hat{\rho}_d^{ij}\bar{Q}_L^i H_2 d_R^j + \hat{\rho}_e^{ij}\bar{L}_L^i H_2 e_R^j, \quad (1.12)$$

where $\tilde{H}_i^a = \epsilon_{ab}H_i^{b*}$ and the $SU(2)$-doublet indices have been suppressed. The right-handed singlets are given by

$$u_R = \{u_R, c_R, t_R\}, \quad (1.13)$$

$$d_R = \{d_R, s_R, b_R\}, \quad (1.14)$$

$$e_R = \{e_R, \mu_R, \tau_R\}, \quad (1.15)$$

and the left-handed $SU(2)$ doublets are given by

$$Q_L = \left\{ \begin{pmatrix} u_L \\ d_L \end{pmatrix}, \begin{pmatrix} c_L \\ s_L \end{pmatrix}, \begin{pmatrix} t_L \\ b_L \end{pmatrix} \right\} \text{ and} \quad (1.16)$$

$$L_L = \left\{ \begin{pmatrix} \nu_L^e \\ e_L \end{pmatrix}, \begin{pmatrix} \nu_L^\mu \\ \mu_L \end{pmatrix}, \begin{pmatrix} \nu_L^\tau \\ \tau_L \end{pmatrix} \right\}. \quad (1.17)$$

Only the Yukawa couplings of H_1 are responsible for generating the fermion masses. Once the mass matrix is diagonalised, the $\hat{y}$ matrices are also diagonalised and do not contribute to the tree-level FCNCs. This transformation still leaves the Higgs doublets in the Higgs basis. After diagonalisation, $\mathcal{L}_Y$ becomes

$$\mathcal{L}_Y = -\frac{1}{\sqrt{2}} \sum_{\substack{\phi=h,H,A \\ f=u,d,e}} y_{\phi ij}^f \bar{f}_i \phi P_R f_j + h.c. \quad (1.18)$$

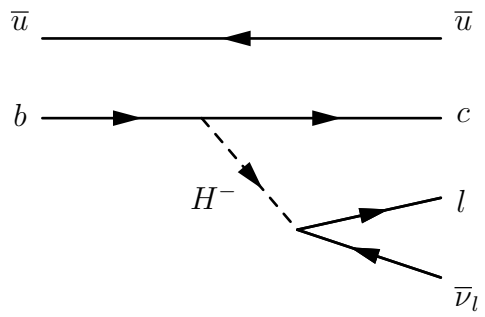

Figure 1.1: Feynman diagram for $B^- \to Dl\bar{\nu}_l$, where the quark composition of B^- is $\{\bar{u}b\}$ and that of D is $\{\bar{u}c\}$.

where

$$y^f_{hij} = \frac{\sqrt{2}m^i_f}{v}\delta_{ij}, \tag{1.19}$$

$$y^f_{Hij} = \rho^{ij}_f, \tag{1.20}$$

$$y^f_{Aij} = \rho^{ij}_f \times \begin{cases} +i, & f = u \\ -i, & f = d, e \end{cases} \tag{1.21}$$

and $P_R = (1+\gamma_5)/2$, $\rho_{u,d,e} = L^\dagger_{u,d,e}\hat{\rho}_{u,d,e}R_{u,d,e}$ and $V_{CKM} = L^\dagger_u L_d$. The relevant part of the Lagrangian for $b \to cl\nu$ processes is

$$\mathcal{L} = -\bar{\nu}(U^\dagger_\nu \rho_e)H^+ P_R e - \bar{u}(V\rho_d P_R - \rho^\dagger_u V P_L)H^+ d + h.c., \tag{1.22}$$

where $U_\nu = L^\dagger_\nu L_e$ is the PMNS matrix. From here onwards, the replacement $U_\nu \nu \to \nu$ is made, where ν indicates the initial flavour eigenstate, since neutrino oscillations are not important in these processes. The new contributions to $B \to D/D^*\tau\nu$ can be mediated by the charged Higgs bosons $H^\pm$ for non-zero $\rho^{i\tau}_e$. The Feynman diagram for the $B^- \to Dl\bar{\nu}_l$ is shown in Fig. 1.4. Since there is an excess of τ final states in the charged B decays, $\rho^{\tau\tau}_e$

is the optimal matrix element for fitting these anomalies. Hence, we take $\rho_e^{\tau\tau}$, henceforth referred to as $\rho^{\tau\tau}$ to be non-zero and the remaining elements of ρ_e to be negligible. Then, $H^{\pm}$ can be integrated out to produce the following effective Lagrangian:

$$\mathcal{L}_{eff} = -\frac{4G_F}{\sqrt{2}} V_{cb}[(C_{S_L}(\bar{c}_R b_L)(\bar{l}_R \nu_L) + C_{S_R}(\bar{l}_R \nu_L)(\bar{C}_L b_R)], \tag{1.23}$$

where G_F is the Fermi constant, V_{cb} is the Cabibbo-Kobayashi-Maskawa (CKM) matrix element, and C_{S_L} and C_{S_R} are the new physics scalar couplings or Wilson coefficients. Now, the quantities $\mathcal{R}_D$ and $\mathcal{R}_{D^{(*)}}$ are functions of these scalar couplings [18].

$$\frac{\mathcal{R}_D}{\mathcal{R}_D^{\rm SM}} = 1 + 1.037R^2 \mid C_{S_L} + C_{S_R} \mid^2 + 1.504R\,\mathcal{R}e[C_{S_L}^* + C_{S_R}^*], \tag{1.24}$$

$$\frac{\mathcal{R}_{D^*}}{\mathcal{R}_{D^*}^{\rm SM}} = 1 + 0.037R^2|C_{S_L} - C_{S_R}|^2 + 0.114R\,\mathcal{R}e[C_{S_L}^* - C_{S_R}^*], \tag{1.25}$$

where $R = 1.46$ is the effect of the renormalisation group evolution of the Wilson coefficients as shown in [19], and we assume that C_{S_L} and C_{S_R} are real to reduce the number of free parameters in the Lagrangian and make the model simpler.

Chapter 2

Complementary constraints

Now that the basic structure of the model has been established, the motivations for considering this model in particular as well as experiments that put constraints on it are discussed in more detail in this chapter to explore the validity of the model.

2.1 Charged Higgs boson mediated processes

There have been continued and consistent observations of deviations in branching ratios in multiple decay channels of the $b \to cl\nu$ processes as well as an excess in τ final states compared to e, μ states in pp collisions that is larger than predicted from phase space effects. In recent years, the LHCb [2], BaBar [3], and Belle [4] collaborations have found significant deviations in the ratios of branching fractions, $\mathcal{R}_D$ and $\mathcal{R}_{D^{(*)}}$, also known as Lepton Flavour Universality Violating (LFUV) observables, in $b \to cl\nu$ processes, defined by

$$\mathcal{R}_X = \frac{\mathcal{B}(B \to X\tau\bar{\nu})}{\mathcal{B}(B \to X(e,\mu)\bar{\nu})}. \tag{2.1}$$

Other LFUV variables that involve the quark-level process $b \to cl\nu$ are

$$\mathcal{R}_{J/\psi} = \frac{\mathcal{B}(B_c \to J/\psi\tau\bar{\nu})}{\mathcal{B}(B_c \to J/\psi(e,\mu)\bar{\nu})} \tag{2.2}$$

and

$$\mathcal{R}_{\Lambda_c} = \frac{\mathcal{B}(\Lambda_b \to \Lambda_c^+\tau\bar{\nu})}{\mathcal{B}(\Lambda_b \to \Lambda_c^+(e,\mu)\bar{\nu})} \tag{2.3}$$

which have been measured by the LHCb in recent years. However, since these last two quantities are more subject to hadronic uncertainties than the LFUV ratios they have been omitted from this analysis for the time being.

The experimental measurements for these quantities as well as their SM values is tabulated below.

Quantity	SM value	Experimental world average
R_D [5]	0.298 ± 0.004	0.357 ± 0.029
R_{D^*} [5]	0.254 ± 0.005	0.284 ± 0.012
$R_{J/\psi}$ [20]	0.258 ± 0.004	0.71 ± 0.17 (stat.) ± 0.18 (syst.)
R_{Λ_c} [21]	0.324 ± 0.004	0.242 ± 0.026 (stat.) ± 0.040 (syst.) ± 0.059

Other non-LFUV observable-measurements that also exhibit deviations from the SM and can be used to constrain the model considered in this work include the τ lepton polarisation fraction, $P_\tau^{D^*}$, and the longitudinal polarisation fraction of the D^* meson, $F_L^{D^*}$, given by

$$P_\tau^{D^*} = \frac{\Gamma^+(B \to D^*\tau\bar{\nu}_\tau) - \Gamma^-(B \to D^*\tau\bar{\nu}_\tau)}{\Gamma(B \to D^*\tau\bar{\nu}_\tau)} \quad \text{and} \tag{2.4}$$

$$F_L^{D^*} = \frac{\Gamma(B \to D_L^*\tau\bar{\nu}_\tau)}{\Gamma(B \to D^*\tau\bar{\nu}_\tau)} \tag{2.5}$$

respectively, where $\Gamma^\pm$ are the decay rates with a τ helicity of $\pm 1/2$. The experimental measurements and SM values for these are shown below.

Quantity	SM value	Experimental value
$P_\tau^{D^*}$	-0.497 ± 0.013 [22]	-0.38 ± 0.51 (stat.) $^{+0.21}_{-0.16}$ (syst.) [23]
$F_L^{D^*}$	0.46 ± 0.04 [24]	$0.60 \pm 0.08 \pm 0.035$ [25]

Additionally, the lifetime of the B_c meson should also impose a constraint on the branching ratio, $\mathcal{B}(B_c \to \tau\bar{\nu})$ since this quantity cannot be greater than the total decay width of B_c. This in turn imposes constraints on the Wilson coefficients mentioned above. $\mathcal{B}(B_c \to \tau\bar{\nu})$ has not yet been measured, however the LEP experiment has imposed the requirement that it be less than or equal to 10% [26]. According to the SM, the lifetime of the B_c meson has been computed to be $\tau_{B_c} = 0.52^{+0.18}_{-0.12}$ ps [27, 28], which is in good agreement with the experimentally obtained value of $\tau_{B_c} = 0.507(9)$ ps [29]. However, again, due to their greater susceptibility to hadronic uncertainties, these quantities been omitted from our analysis for now.

Apart from this, the pair-production of H^+ and H^- is also constrained from the cross-section of proton-proton collisions resulting in $\tau\tau$ final states in searches for charged Higgs bosons measured by CMS [30].

2.2 SM-like Higgs boson mediated processes

The other relevant observables for the model are through processes that could be mediated by a lighter neutral SM-like Higgs boson. CMS observed a possible excess in $\tau\tau$ final states in searches for additional Higgs bosons with local p-values equivalent to around 3σ at 0.1 TeV [12]. Besides this, ATLAS [31] and CMS [9] have reported an excess of diphoton events that are also indicative of a neutral Higgs with a mass around 95 GeV [10, 11]. Hence, hypothetically, these processes can both be mediated by H, thereby adding an extra channel, compared to the SM, for ditau and diphoton production respectively.

2.3 Model independent analysis

Previous studies have explored the possibility of new physics (NP) contributions to the anomalies mentioned above by making use of a model-independent effective field theory (EFT) approach. One such work is [7], the focus of which was to include the new experimental data from the Belle collaboration [32] on the measurement of R_{D^*} using the semileptonic tag and on the longitudinal polarisation of D^*, $F_L^{D^*}$ into the analysis in addition to the existing data on $R_{D^*}, R_{J/\psi}, P_\tau^{D^*}$, and F_L^{D*}. They find that though the new Belle data on R_{D^*} using the semileptonic tag reduces the tension with the SM predictions compared to the previous average computed by the HFLAV, it doesn't do so by much still leaving a tension of 2.7σ. Performing two types of fits, first, one- and two-parameter fits of the Wilson coefficients to the 2019 HFLAV average of R_D and R_{D^*}, and secondly, a global fit of all NP operators (only taking into account interactions associated with left-handed neutrinos) to the whole data i.e. $R_{D^*}, R_{J/\psi}, P_\tau^{D^*}$, and F_L^{D*}. Upper bounds derived from the lifetime of the B_c meson were also included in the analysis. From the first fit, it was found that NP models consisting of left-handed currents and tensor operators were favoured while those based on purely right-handed currents were disfavored by the LHC data. Moreover, models with only scalar operator contributions were found to be inconsistent with both LHC and B_c meson constraints. Overall, the second fit which included all the available data favoured similar regions to the first one with the added effect of ruling out large values of the Wilson coefficients. However, a significant limitation of the analysis performed in [7] is that if the NP particles responsible for mediating these processes have mass scales lower than about 2 TeV (which is the case for our model, where we conjecture the mediating NP particle, H^+ to be about 95 GeV), then the EFT approach used breaks down and the LHC bounds are rendered invalid. Hence, to get more reliable information relevant to the model considered in this project, the results of an alternative approach to a model-independent analysis is presented below.

The remaining portion of this section is primarily based on the analysis carried out in [8]. To get an understanding of the effect of each Wilson Coefficient on the observables, χ^2 fits of the scalar couplings, C_{S_L} and C_{S_R}, were performed to the measured observables, R_D and R_{D^*} for the following scenarios:

- Case (i): Assuming that C_{S_L} and C_{S_R} are both real and setting one (C_{S_L} or C_{S_R}) equal to zero to investigate the effect of the other on the observables.
- Case (ii): Assuming that C_{S_L} and C_{S_R} are complex and setting one (C_{S_L} or C_{S_R}) equal to zero to investigate the effect of the other.
- Case (iii): Varying the values of both scalar couplings to investigate their combined effect.

Using these, the following best fit values were obtained.

Case	(i)	(ii)	(iii)
C_{S_L}	0.15	$-0.67 - i\ 0.84$	$-0.37 + i\ 0$
C_{S_R}	0.16	$0.16\ -i\ 6.4\ \times 10^{-6}$	$0.48\ +\ i\ 0$

The implications of these best fit values on the $R_D - R_{D^*}$ plane are presented in fig. 2.1. As can be seen from the leftmost and central plots, for both real and complex choices of C_{S_L} and C_{S_R}, the best fit values lie within 2σ of the experimental results, although in the case of C_{S_L}, the choice of complex values rather than real ones is in better agreement. In the rightmost plot, the relevant data point for us is the one corresponding to case (iii) from above, where all couplings except C_{S_L} and C_{S_R} were set to zero and C_{S_L} and C_{S_R} were varied simultaneously. This corresponds to the green triangle labelled (C^S_{LL}, C^S_{RL}).

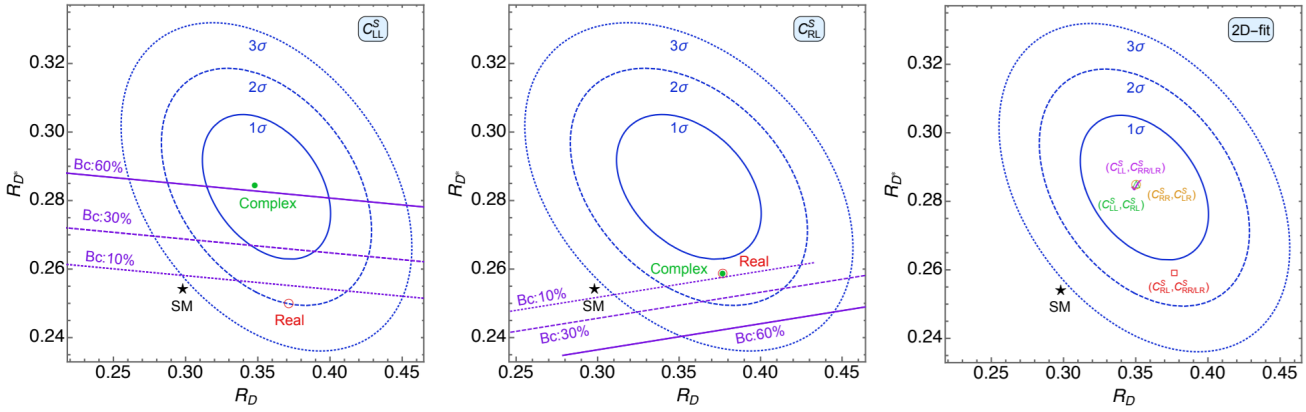

Figure 2.1: Permitted regions in the $R_D - R_{D^*}$ plane using the best fit values of the Wilson coefficients [8]. The solid, dashed, and dotted lines in blue indicate the 1σ, 2σ, and 3σ contours of the experimental results respectively. The red circle and green point denote the best fit values of the scalar couplings assuming them to be real and complex respectively. The SM prediction for R_D and R_{D^*} is denoted by the black star. The solid, dashed, and dotted lines in purple represent $\mathcal{B}(B_c \to \tau\bar{\nu}) = 60\%$, 30% (these two scenarios have been considered despite the constraint from LEP mentioned earlier for thoroughness, since they are still reasonable choices), and 10% respectively.

Chapter 3

Analysis

As mentioned before, the recent discovery of the excess in ditatu [12] final states in proton-proton collision searches for additional Higgs bosons, with the largest deviations occurring around a mass of around 95 GeV motivated us to perform a combined analysis of this anomaly together with the persisting flavour anomaly observed in $B \to Dl\bar{\nu}_l$ and $B \to D^* l\bar{\nu}_l$ processes [2, 3, 4]. We wanted to see if these anomalies could be explained using a general type III 2HDM, where the former anomaly could be mediated by a lighter SM-like Higgs boson, H with a mass of around 95 GeV, and the latter two by a positively-charged Higgs boson, H^+ with a similar mass range. Initially, we thought that the 2HDM could also provide a possible explanation for the recent observations of a diphoton excess in new Higgs searches through proton-proton collisions [9, 31]. However, as will be shown below, our analysis showed that the model cannot be used to explain this anomaly.

3.1 $B \to Dl\bar{\nu}_l$ and $B \to D^* l\bar{\nu}_l$ anomalies

We start by determining the Wilson coefficients, $C_{S_L}^{cb}$ and $C_{S_R}^{cb}$ appearing in the operators of the effective Hamiltonian that are responsible for the interactions required for the $B \to D\tau\nu$ and $B \to D^{(*)}\tau\nu$ processes. This can be done by using (1.24) and (1.25), and the

experimental world average and SM values for R_D and R_{D^*} shown in Table 2.1. Using these, we get the following sets of central values for the Wilson coefficients:

$$\begin{aligned}(C_{S_L}^{cb}, C_{S_R}^{cb}) =&(-1.89, 0.816), (-1.31, 1.39),\\ &(-0.239, -0.834), (0.338, -0.258).\end{aligned} \tag{3.1}$$

Let us label these four sets of values as sets 1, 2, 3, and 4 respectively. Now, in order to translate these into constraints on the couplings, we require the following ansatz which was introduced in [1] relating the up-type and down-type Yukawa matrices, ρ_u and ρ_d, of the new Higgs doublet:

$$\rho_u^\dagger V = \eta U V \rho_d, \tag{3.2}$$

where V is the CKM matrix and and U is a diagonal unitary matrix, where $U_{11} = -1$, and $U_{22} = 1$. U_{33} has not yet been determined by experimental constraints. However, it was noted that if $U_{33} \cong -1$ then U would be a special unitary matrix. This ansatz is referred to as the "charge transformation" mechanism and was motivated by viable solutions of the Wilson Coefficients to fits performed in [33] that suggested such a relation between the Yukawa matrices. It was also supported by bounds deduced from the world average measurement and CKMfitter prediction of the branching ratio $\mathcal{B}(B^+ \to \tau^+\nu)$. However, the main purpose of introducing the ansatz was to give more structure to the couplings of the new Higgs particles than is possible if ρ_u and ρ_d are independent of each other. Additionally, through the introduction of this ansatz, it was possible to allow for generic Yukawa couplings to the new Higgs doublet without the need for introducing a specific mechanism to supress FCNCs. It was shown in [1], how FCNCs can simply be avoided due to the negligible values taken up by the problematic coupling constants. Although the model does not have any symmetries to justify the negligibility of these couplings, it was shown to be free from fine tuning. Furthermore, observables such as meson oscillations that provide the most stringent

constraints on this ansatz were computed along with rare decay processes that might also challenge the ansatz and these were found to be consistent with the proposed ansatz.

Now, using

$$\rho_u^\dagger V = \eta U V \rho_d, \tag{3.3}$$

we obtain

$$\eta = 0.432, -1.06, -3.49, 0.763, \tag{3.4}$$

and

$$\rho^{\tau\tau}\rho^{bb} = \frac{4G_{\rm F}m_\pm^2}{\sqrt{2}}C_{S_R}^{cb}. \tag{3.5}$$

It should be noted here that using the experimental values for R_D and R_{D^*} and the proposed ansatz, we are only able to constrain the product $\rho^{\tau\tau}\rho^{bb}$, and not the coupling constants separately.

3.2 Diphoton cross-section

The diphoton cross-section is given by

$$\sigma(pp \to H \to \gamma\gamma) = \sigma(pp \to H) \times \frac{\Gamma(H \to \gamma\gamma)}{\Gamma_H}. \tag{3.6}$$

The total decay width of the new CP-even neutral Higgs, H is dominated by $b\bar{b}$ and $\tau\bar{\tau}$ decay at tree level due to the dominance of the respective coupling constants so that

$$\Gamma_H = \frac{m_H}{16\pi}\left[3(\rho^{bb})^2 + (\rho^{\tau\tau})^2\right]. \tag{3.7}$$

The partial decay to $\gamma\gamma$ occurs via t, b, and τ at one loop, which should have the same expression as for the SM Higgs since the physics is all the same with the only difference being the different coupling constants between the lighter Higgs, H and the fermions. Hence, we can use the following expression from [34]

$$\Gamma(H \to \gamma\gamma) = \frac{\alpha^2 m_H^3}{512\pi^3} \left| \frac{4\rho^{tt} A_t(\tau_t)}{3m_t} + \frac{\rho^{bb} A_b(\tau_b)}{3m_b} + \frac{\rho^{\tau\tau} A_b(\tau_\tau)}{m_\tau} \right|^2, \tag{3.8}$$

replacing $1/v$ with $\rho^{ii}/(\sqrt{2}m_i)$ to adapt it to our model. In all equations where m_b appears, we took it to be 2.9 GeV [35], the value at the weak scale. Now, in order to compute $\sigma(pp \to H)$, we can use the parton model which is generally used to study high-energy collisions of hadrons.

It was observed in the 60s that when a hadron moves at a speed close to the speed of light, as is the case in high-energy collisions, it is better described as containing an infinite number of particles — quarks, gluons, and even antiquarks (due to virtual processes such as the quark loop diagram contributing to the gluon jet function) called partons — with a wide range of momenta [36]. This is in contrast to the quark model where hadrons are thought of as quantum bound states of quarks, which is a more appropriate picture for hadrons that are moving at non-relativistic speeds. For our case, the dominating processes that contribute to H-production in proton-proton collisions are H-production through $b\bar{b}$ and gluon-fusion. The way this occurs is each proton contributes a quark (or antiquark) which contains some fraction x of the proton's total momentum, p. Then we can define a

new Mandelstam variable, $\hat{s}$ for the partons given by

$$\begin{aligned}\hat{s} &= (x_1 p_1 + x_2 p_2)^2 \\ &= x_1^2 p_1^2 + x_2^2 p_2^2 + 2x_1 x_2 p_1 p_2 \\ &= (x_1^2 + x_2^2) m_b^2 + x_1 x_2 (s - 2m_b^2) \\ &\approx x_1 x_2 s, \end{aligned} \tag{3.9}$$

since $s = 13\ \text{TeV} \gg m_b^2$. The parton-level cross-section is given by

$$\begin{aligned}\hat{\sigma}(b\bar{b} \to H) = \frac{|\mathcal{M}|^2}{4\sqrt{\hat{s}} p_b} \hat{I}_1 &= \frac{|\mathcal{M}|^2}{4\sqrt{\hat{s}} p_b} \cdot 2\pi \int \frac{d^3 p}{2E} \delta^{(3)} (\overrightarrow{p} - \overrightarrow{p}_1 - \overrightarrow{p}_2)\, \delta\left(E - \sqrt{\hat{s}}\right) \\ &= \frac{|\mathcal{M}|^2}{4\sqrt{\hat{s}} p_b} \cdot \frac{\pi}{\sqrt{\hat{s}}} \delta\left(\sqrt{(\overrightarrow{p}_1 + \overrightarrow{p}_2)^2 + m_H^2} - \sqrt{\hat{s}}\right). \end{aligned} \tag{3.10}$$

Substituting in the expression for the matrix element for the tree-level process $b\bar{b} \to H$ which is straightforward to compute, in the centre-of-mass frame, we get

$$\hat{\sigma}(b\bar{b} \to H) = \frac{\pi (\rho^{bb})^2}{36} \delta(\hat{s} - m_H^2). \tag{3.11}$$

In order to see how this contributes to $\sigma(pp \to H)$, we need the probability densities for the b and $\bar{b}$ to carry fractions x_1 and x_2 respectively of the protons' total momenta. These are given by parton distribution functions (PDF), $f_b(x, Q)$, where Q is the energy-scale of the process being considered, which in our case is the mass of the SM-like lighter Higgs boson, m_H. These functions have been determined through various experiments and in this thesis, the MSTW PDF package [37] for Mathematica was used to access them for the following computations. To get $\sigma(pp \to H)$, we integrate over all possible values of fractions for each

parton as follows:

$$\sigma(pp \to H) = \int_0^1 dx_1 f_b(x_1, m_H) \int_0^1 dx_2 f_{\bar{b}}(x_2, m_H) \hat{\sigma}(b\bar{b} \to H) \tag{3.12}$$

$$= \frac{\pi(\rho^{bb})^2}{36} \int_0^1 dx_1 f_b(x_1, m_H) \int_0^1 dx_2 f_{\bar{b}}(x_2, m_H) \delta(\hat{s} - m_H^2) \tag{3.13}$$

$$= \frac{\pi(\rho^{bb})^2}{36} \int_0^1 dx_1 f_b(x_1, m_H) \int_0^1 dx_2 f_{\bar{b}}(x_2, m_H) \delta(x_1 x_2 s - m_H^2) \tag{3.14}$$

$$= \frac{\pi(\rho^{bb})^2}{36} \int_0^1 dx_1 f_b(x_1, m_H) f_{\bar{b}} \left(\frac{m_H^2}{x_1 s}, m_H \right) \Theta \left(1 - \frac{m_H^2}{x_1 s} \right) \frac{1}{x_1 s} \tag{3.15}$$

$$= \frac{\pi(\rho^{bb})^2}{36s} \int_{m_H^2/s}^1 \frac{dx_1}{x_1} f_b(x_1, m_H) f_{\bar{b}} \left(\frac{m_H^2}{x_1 s}, m_H \right), \tag{3.16}$$

where in the fourth step, the step-function ensures that $x_2 \leq 1$. The PDFs diverge for small x. So, using the function xf is numerically more convenient to work with and hence we rewrite the above as

$$\sigma(pp \to H) = \frac{\pi(\rho^{bb})^2}{36 m_H^2} \int_{m_H^2/s}^1 \frac{dx_1}{x_1} [x_1 f_b](x_1, m_H) [x_1 f_{\bar{b}}] \left(\frac{m_H^2}{x_1 s}, m_H \right), \tag{3.17}$$

where

$$\mathcal{L}_i = \int_{m_H^2/s}^1 \frac{dx}{x} [x f_i](x, m_H) [x f_i] \left(\frac{m_H^2}{xs}, m_H \right) \tag{3.18}$$

is known as the parton luminosity factor. Now, the most dominant contribution to $\sigma(pp \to H)$ comes from gluon fusion followed by the $b\bar{b}$ contribution. So, the full expression for $\sigma(pp \to H)$ is actually given by

$$\sigma(pp \to H) = \frac{\pi(\rho^{bb})^2}{36 m_H^2} \mathcal{L}_b + \hat{\sigma}_{LO}(gg \to H) \mathcal{L}_g, \tag{3.19}$$

where [38],

$$\hat{\sigma}_{LO}(gg \to H) = \frac{\alpha_s^2(\mu)}{2048\pi} \left| \frac{\rho^{tt} A_t(\tau_t)}{m_t} + \frac{\rho^{bb} A_b(\tau_b)}{m_b} \right|^2. \tag{3.20}$$

Here, $\tau_f = m_H^2/(4m_f^2)$,

$$A_f(\tau_f) = \frac{2}{\tau_f^2}[\tau_f + (\tau_f - 1)f(\tau_f)], \tag{3.21}$$

and

$$f(\tau_f) = \begin{cases} \arcsin^2(\sqrt{\tau_f}), & \tau_f \leq 1 \\ -\frac{1}{4}\left[\log\left(\frac{1+\sqrt{1-\tau_f^{-1}}}{1-\sqrt{1-\tau_f^{-1}}}\right) - i\pi\right]^2, & \tau_f > 1. \end{cases} \tag{3.22}$$

To compare the predictions made by the model to the data, the product of the production cross section of an SM-like Higgs boson of mass m_H and its branching fraction to photons was used from Fig. 5 of [12]. The corresponding plots of $\sigma(pp \to H \to \gamma\gamma)$ for the model and that obtained from [12] are shown in Fig. 3.1. As shown, the diphoton signal we obtained was too weak to describe the observed diphoton excess. The reason for this can be explained as follows. In our model, the diphoton final states are only produced through loop contributions which are competing with the tree-level $t\bar{t}, b\bar{b}$, and $\tau\bar{\tau}$ final states. We cannot switch off these couplings because we need them to explain the flavour anomaly in the B meson decay. The couplings ρ^{bb}, and $\rho^{\tau\tau}$ are required in order to get the desired value of the Wilson coefficients, $C_{S_R}^{cb}$ and $C_{S_L}^{cb}$. Additionally, for non-zero Wilson coefficients, η must be non-zero and hence ρ^{tt} cannot be switched off either. Hence, the tree-level decays are always much faster than the diphoton decays, making it impossible to achieve the desired branching ratio.

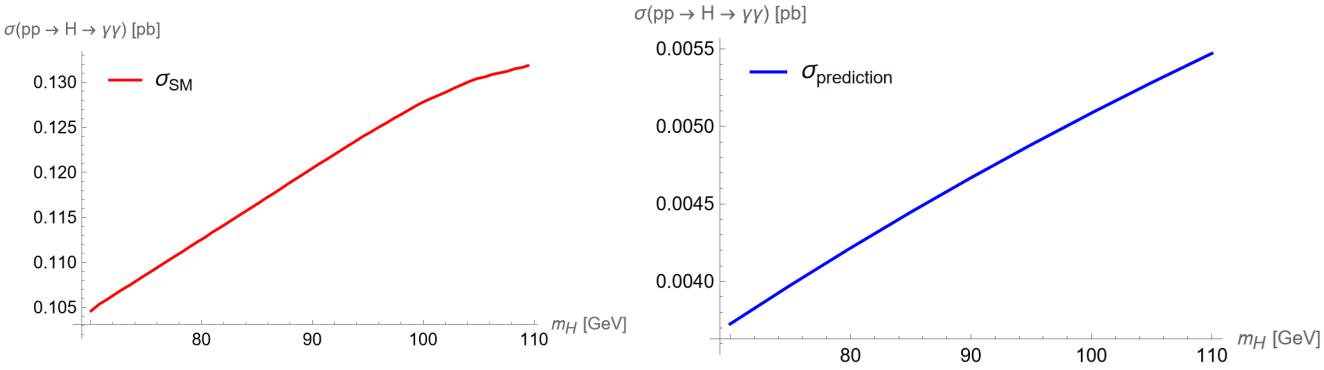

Figure 3.1: $\sigma(pp \to H \to \gamma\gamma) = \sigma(pp \to H) \times \mathcal{B}(H \to \gamma\gamma)$ as for an SM-like Higgs boson of mass m_H using [12] on the left, and that using our model (assuming SM values for the couplings) on the right.

3.3 Ditau cross-section

The cross-section for the ditau final state process can be calculated by replacing $\Gamma(H \to \gamma\gamma)$ in (3.6) by $\Gamma(H \to \tau\bar{\tau})$, where

$$\Gamma(H \to \tau\bar{\tau}) = \frac{m_H}{16\pi}(\rho^{\tau\tau})^2, \tag{3.23}$$

which results in a branching fraction of ~ 1. Hence, the cross-section is now just a function of ρ^{bb} and m_H. To illustrate this, the cross-section is plotted as a function of ρ^{bb} in Fig. 3.2 for three different values of m_H. To narrow down the parameter space for the couplings, we can interpolate the data for the 95% confidence level upper limit of the expected and observed ditau cross-section from CMS [12] to get the upper limit of ρ^{bb} as a function of m_H. This is shown in Fig. 3.3.

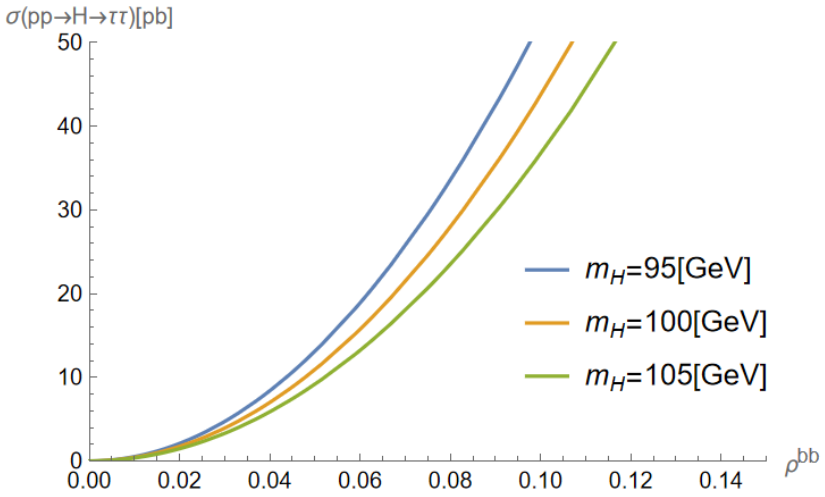

Figure 3.2: $\sigma(pp \to H \to \tau\tau^-)$ as a function of ρ^{bb} for $m_H = 95$ GeV, 100 GeV, 110 GeV.

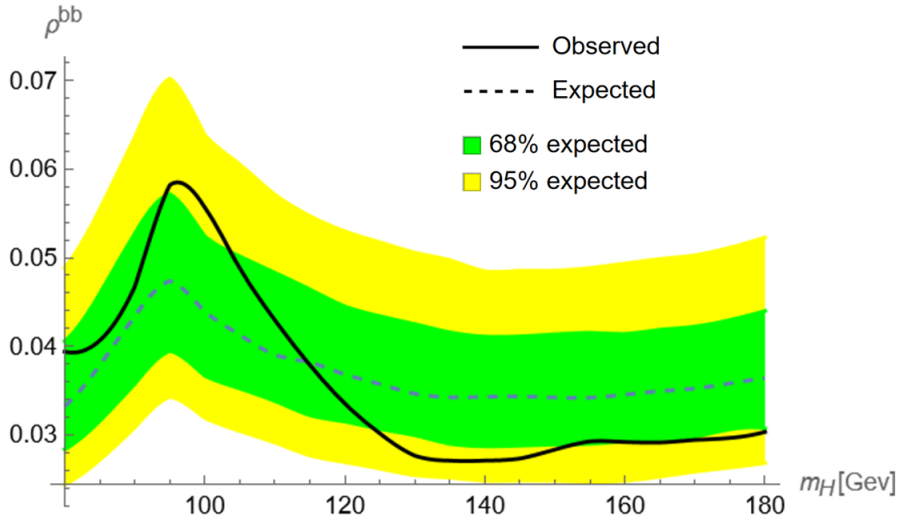

Figure 3.3: 95% confidence level upper limit of ρ^{bb} as a function of m_H as deduced from the CMS expected and observed 95% CL upper limits on the product of the cross sections ggH and $b\bar{b}H$ and branching fraction for decay into $\tau^+\tau^-$ final states [12].

Then we can use (3.5) to obtain the lower limit of $\rho^{\tau\tau}$ in terms of m_H and $m_\pm$. In order to do this, we need to choose a set of values for the product of the couplings, $\rho^{bb}\rho^{\tau\tau}$ corresponding to (3.1) from above. To do this, we decided to plot the cross-section as a function of ρ^{bb} for $m_H = 95$ GeV. This is shown in Fig. 3.4.

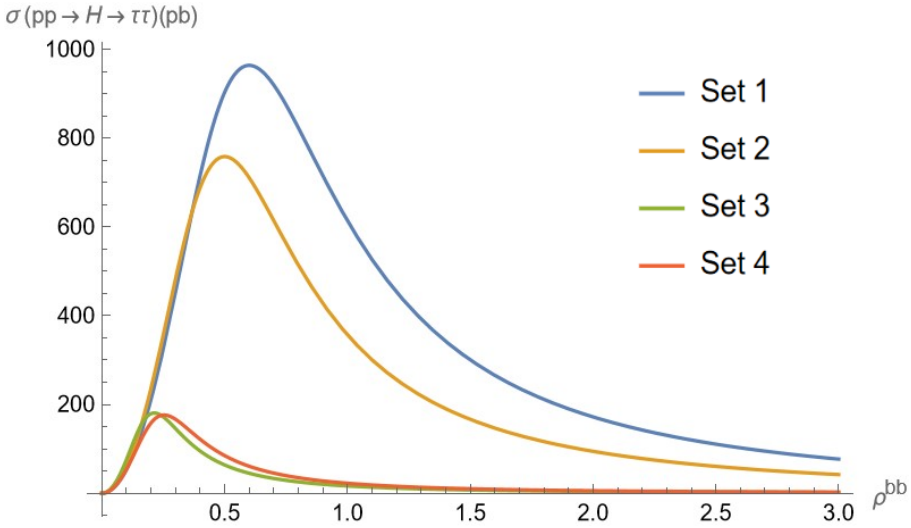

Figure 3.4: $\sigma(pp \to H \to \tau\tau^-)$ as a function of ρ^{bb} for $m_H = 95$ GeV for the four different sets of values for the Wilson coefficients obtained in (3.1).

Now, from Fig. 10 in [12], we see that in the mass range $60 \leq m_H \leq 3500$ GeV, the highest upper limit attained by $\sigma(ggH) \times \mathcal{B}(H \to \tau^+\tau^-)$ and $\sigma(b\bar{b}H) \times \mathcal{B}(H \to \tau^+\tau^-)$ together is ~ 50 pb. As we can see, the first two sets of values for the fits give us far too large values for the cross-section, so these can be ruled out immediately. In order to choose between the remaining two sets, we can look at the value for η. For the fourth set of values, $\eta = 0.763$ and in [1], $\eta \sim 0.8$ was shown to avoid undesirable FCNCs while being consistent with R_{D^*} anomalies. Hence, we proceed by plugging in the fourth set of values into (3.5) to get the lower limit of $\rho^{\tau\tau}$ as a function of m_H and $m_\pm$. This is plotted in Fig. 3.5.

Now we discuss an alternative equally valid way of calculating the cross-section for the $pp \to H \to \tau\tau$ process. The purpose of doing this is to see if the cross-section computed this way is able to attain values for the cross-section that are consistent with limits obtained by CMS [12], to corroborate the plausibility of our model. This can be done by using the relation

$$\sigma_{\text{LO}}(gg \to H) = \frac{G_F \alpha_S^2(\mu)}{288\sqrt{(2)}\pi} \left| \frac{3}{4} \sum_q A_{1/2}^H(\tau_q) \right|^2 \tag{3.24}$$

for the SM Higgs production through gluon fusion, which is the dominant production for

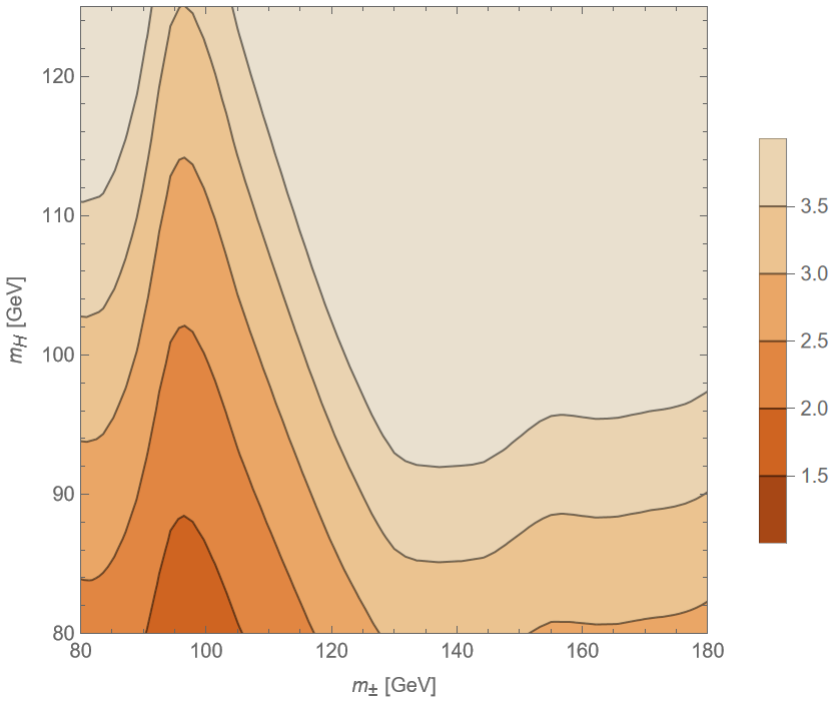

Figure 3.5: Contours of lower limit of $\rho^{\tau\tau}$ as a function of m_H and $m_\pm$.

the lighter Higgs in our model too (as was also observed when looking at the contributions of the $b\bar{b}$ vs the gluon fusion process to the total production cross-section $\sigma(pp \to H)$ in the previous section). Now, the functions $A(\tau)$ are suppressed by τ_f which is further suppressed by the square of the mass of the corresponding fermion. Since $m_t \gg m_b$, we can neglect the contribution from the b-quark in the loop. Hence, the only difference between the expressions for the cross-sections of the SM Higgs and the lighter one is the factor of $G_F = 1/(\sqrt{2}v^2)$, which should be replaced by $(\rho^{ii})^2/(2m_i^2)$ for the 2HDM case. Hence,

$$\sigma_{\text{2HDM}}(pp \to H \to \tau\tau^-) = \sigma_{\text{2HDM}}(pp \to H) = \left(\frac{\rho^{tt}_{,\text{2HDM}}}{\rho^{tt}_{,\text{SM}}}\right)^2 \sigma_{\text{LO, SM}}(gg \to h), \tag{3.25}$$

where $\sigma_{LO,SM}(gg \to h)$ can be obtained by interpolating the data from the Higgs Working Group, WG1 [39]. Using this, we obtain $\sigma_{\text{2HDM}}(pp \to H \to \tau\tau^-)$ as a function of ρ^{tt} and m_H. This is plotted in Fig. 3.6. Again compairing to the combined limit on $\sigma(ggH)\mathcal{B}(H \to$

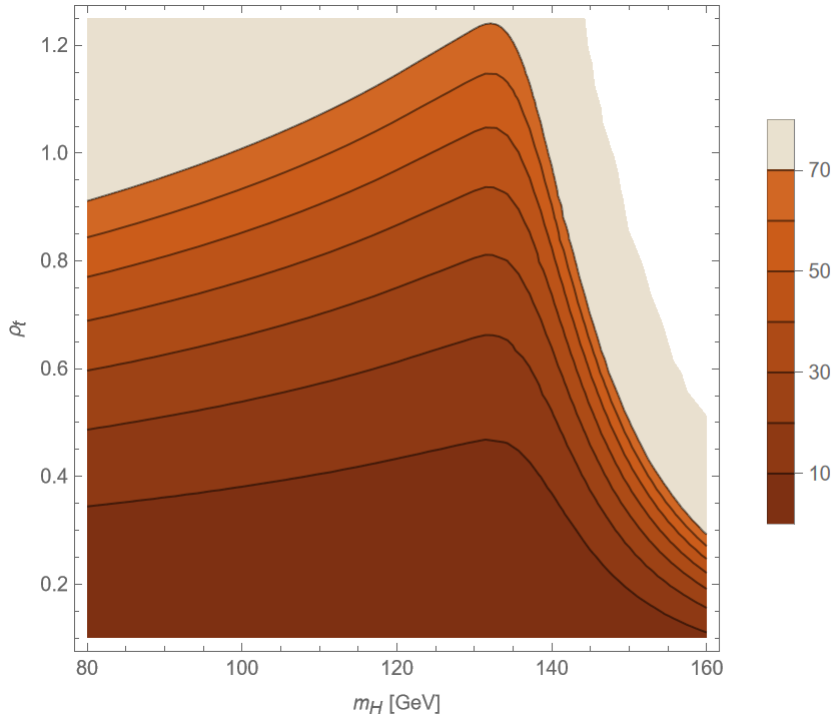

Figure 3.6: $\sigma(pp \to H \to \tau\tau)$ in units of pb as a function of m_H for different values of ρ^{tt}.

$\tau^+\tau^-) + \sigma(b\bar{b}H)\mathcal{B}(H \to \tau^+\tau^-)$ from Fig. 10 in [12], we see that a non-negligible part of the parameter space leads to values of the cross-section that are compatible with the experimental findings of CMS. For a mass of 95 GeV of the lighter SM-like Higgs, for instance, $\rho^{tt} \leq 0.8$ is able to explain the ditau excess. In summary, although the model is unable to explain the diphoton excess observed at 95 [GeV], it is able to do so simultaneously with the charged B decay flavour anomalies and ditau excess at the same mass.

3.4 H^+H^- pair production cross-section

Finally, there are bounds on the pair-production of H^+ and H^- from the cross-section of proton-proton collisions resulting in $\tau\tau$ final states in searches for charged Higgs bosons measured by CMS [30]. In order to compare the predictions from the model to this data we

can use the following equation:

$$\sigma(pp \to H^{\pm} \to \tau^{\pm}\nu_{\tau}) = \sigma(pp \to H^{\pm}) \times \mathcal{B}(H^{\pm} \to \tau^{\pm}\nu_{\tau}), \tag{3.26}$$

where $\mathcal{B}(H^{\pm} \to \tau^{\pm}\nu_{\tau}) = 1$ in the model due to the dominance of $\rho^{\tau\tau}$ over other couplings. In order to compute $\sigma(pp \to H^{\pm})$, we used the MADGRAPH5_aMC@NLO event generator [40, 41]. Using this, the cross-section was obtained as a function of $m_{H^{\pm}}$. This is plotted in Fig. 3.7 together with the upper limit on the cross-section observed by CMS [30].

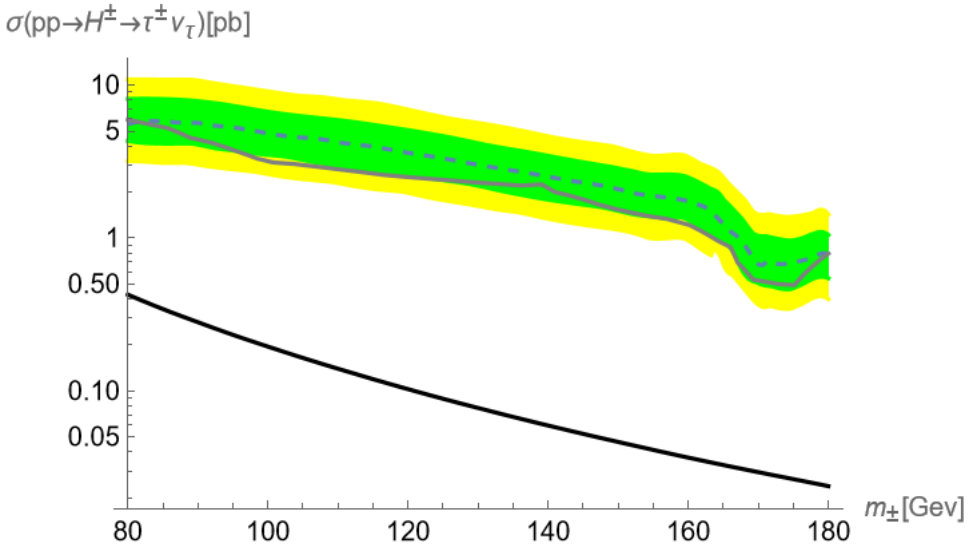

Figure 3.7: 95% CL exclusion limits on $\sigma(pp \to H^{\pm} \to \tau^{\pm}\nu_{\tau})$ as a function of $m_{H^{\pm}}$. The upper cross-section limit observed by CMS [30] is represented by the solid gray line, the expected limit assuming only standard model processes is denoted by the dotted line. The green and yellow bands represent the one and two sigma intervals from the expected limit respectively. The black line represents the cross-section obtained through simulations using MadGraph.

As we can see, the model produces a cross-section that is well within the observed upper limit and is hence permitted by the experimental data.

Conclusion

Although the SM has had huge success in correctly describing what we observe in particle physics experiments, there have long been some experimental observations that it is fundamentally unable to explain, making it an incomplete theory. One of the simplest extensions to the SM is the 2HDM which has the potential to resolve some of these problems with the SM. It has been shown before that the most general form of this model is compatible with anomalies observed in $B \to Dl\nu_l$ and $B \to D^* l\nu_l$ decays. In my thesis I explore if the model is simultaneously compatible with other experimental anomalies as well, namely an excess in $\gamma\gamma$ and $\tau\tau$ final states in proton-proton collisions in searches for additional Higgs bosons. I find that the model produces too weak a cross-section to explain the diphoton excess. However, comparing Fig. (3.6) with bounds for the upper limits of $\sigma(pp \to H \to \tau\tau)$ from [12], it was found that there is a section of parameter space where the model is consistent with the observed ditau excess. Additionally, by performing a combined analysis of the charged B decay anomalies and the ditau excess, an upper limit on the new Yukawa coupling between H and b and a lower one on the Yukawa coupling between H and τ were obtained as a function of the mass of H. It was further shown that the model is consistent with bounds on charged Higgs pair-production from $pp \to \tau^{\pm}\nu_\tau$ processes. Overall, it was found that although the data does not have a preference for this model, it does not rule it out either.

In future work, the $R_{J/\psi}$, R_{Λ_c}, $P_\tau^{D^*}$, and $F_L^{D^*}$ constraints could be taken into account to further constrain the parameter space or rule out the model. Additionally, QCD corrections

of the cross-sections computed in this paper can also be taken into account to produce a more accurate comparison to experimental data.

References

[1] James M. Cline. "Scalar doublet models confront τ and b anomalies". In: *Phys. Rev. D* 93.7 (2016), p. 075017. DOI: 10.1103/PhysRevD.93.075017. arXiv: 1512.02210 [hep-ph].

[2] R. Aaij et al. "Measurement of the Ratios of Branching Fractions $\mathcal{R}(D)$ and $\mathcal{R}(D^*)$". In: *Physical Review Letters* 131.11 (Sept. 2023). ISSN: 1079-7114. DOI: 10.1103/physrevlett.131.111802. URL: http://dx.doi.org/10.1103/PhysRevLett.131.111802.

[3] J. P. Lees et al. "Measurement of an excess of $\bar{B} \to D^{(*)}\tau^-\bar{\nu}_\tau$ decays and implications for charged Higgs bosons". In: *Physical Review D* 88.7 (Oct. 2013). ISSN: 1550-2368. DOI: 10.1103/physrevd.88.072012. URL: http://dx.doi.org/10.1103/PhysRevD.88.072012.

[4] G. Caria et al. "Measurement of $\mathcal{R}(D)$ and $\mathcal{R}(D^*)$ with a Semileptonic Tagging Method". In: *Physical Review Letters* 124.16 (Apr. 2020). ISSN: 1079-7114. DOI: 10.1103/physrevlett.124.161803. URL: http://dx.doi.org/10.1103/PhysRevLett.124.161803.

[5] "Preliminary average of $R(D)$ and $R(D^*)$ for Summer 2023". In: (2023). URL: https://hflav-eos.web.cern.ch/hflav-eos/semi/summer23/html/RDsDsstar/RDRDs.html.

[6] Syuhei Iguro and Kazuhiro Tobe. "$R(D^{(*)})$ in a general two Higgs doublet model". In: *Nucl. Phys. B* 925 (2017), pp. 560–606. DOI: 10.1016/j.nuclphysb.2017.10.014. arXiv: 1708.06176 [hep-ph].

[7] Rui-Xiang Shi et al. "Revisiting the new-physics interpretation of the $b \to c\tau\nu$ data". In: *JHEP* 12 (2019), p. 065. DOI: 10.1007/JHEP12(2019)065. arXiv: 1905.08498 [hep-ph].

[8] Nilakshi Das, Amit Adhikary, and Rupak Dutta. "Revisiting $b \to c\tau\nu$ anomalies with charged Higgs boson". In: (May 2023). arXiv: 2305.17766 [hep-ph].

[9] Albert M Sirunyan et al. "Search for a standard model-like Higgs boson in the mass range between 70 and 110 GeV in the diphoton final state in proton-proton collisions at $\sqrt{s} = 8$ and 13 TeV". In: *Phys. Lett. B* 793 (2019), pp. 320–347. DOI: 10.1016/j.physletb.2019.03.064. arXiv: 1811.08459 [hep-ex].

[10] Thomas Biekötter, Sven Heinemeyer, and Georg Weiglein. "The CMS di-photon excess at 95 GeV in view of the LHC Run 2 results". In: *Phys. Lett. B* 846 (2023), p. 138217. DOI: 10.1016/j.physletb.2023.138217. arXiv: 2303.12018 [hep-ph].

[11] T. Biekötter, S. Heinemeyer, and G. Weiglein. "The 95.4 GeV di-photon excess at ATLAS and CMS". In: (June 2023). arXiv: 2306.03889 [hep-ph].

[12] A. Tumasyan, W. Adam, et al. "Searches for additional Higgs bosons and for vector leptoquarks in $\tau\tau$ final states in proton-proton collisions at $\sqrt{s} = 13$ TeV". In: *Journal of High Energy Physics* 2023.7 (July 2023). ISSN: 1029-8479. DOI: 10.1007/jhep07(2023)073. URL: http://dx.doi.org/10.1007/JHEP07(2023)073.

[13] John F. Gunion et al. *The Higgs Hunter's Guide*. Vol. 80. 2000. ISBN: 978-0-429-49644-8. DOI: 10.1201/9780429496448.

[14] G.C. Branco et al. "Theory and phenomenology of two-Higgs-doublet models". In: *Physics Reports* 516.1–2 (July 2012), pp. 1–102. ISSN: 0370-1573. DOI: 10.1016/j.physrep.2012.02.002. URL: http://dx.doi.org/10.1016/j.physrep.2012.02.002.

[15] R. D. Peccei and Helen R. Quinn. "CP Conservation in the Presence of Pseudoparticles". In: *Phys. Rev. Lett.* 38 (25 June 1977), pp. 1440–1443. DOI: 10.1103/PhysRevLett.38.1440. URL: https://link.aps.org/doi/10.1103/PhysRevLett.38.1440.

[16] Mark Trodden. *Electroweak Baryogenesis: A Brief Review*. 1998. arXiv: hep-ph/9805252 [hep-ph]. URL: https://arxiv.org/abs/hep-ph/9805252.

[17] K Nakamura and (Particle Data Group). "Review of Particle Physics". In: *Journal of Physics G: Nuclear and Particle Physics* 37.7A (July 2010), p. 075021. DOI: 10.1088/0954-3899/37/7A/075021. URL: https://dx.doi.org/10.1088/0954-3899/37/7A/075021.

[18] Rusa Mandal et al. "The role of right-handed neutrinos in $b \to c\tau\bar{\nu}$ anomalies". In: *JHEP* 08.08 (2020), p. 022. DOI: 10.1007/JHEP08(2020)022. arXiv: 2004.06726 [hep-ph].

[19] Martín González-Alonso, Jorge Martin Camalich, and Kin Mimouni. "Renormalization-group evolution of new physics contributions to (semi)leptonic meson decays". In: *Phys. Lett. B* 772 (2017), pp. 777–785. DOI: 10.1016/j.physletb.2017.07.003. arXiv: 1706.00410 [hep-ph].

[20] Judd Harrison, Christine T.H. Davies, and Andrew Lytle. "$R(J/\psi)$ and $B_c^- \to J/\psi l^- \bar{\nu}_l$ Lepton Flavor Universality Violating Observables from Lattice QCD". In: *Physical Review Letters* 125.22 (Nov. 2020). ISSN: 1079-7114. DOI: 10.1103/physrevlett.125.222003. URL: http://dx.doi.org/10.1103/PhysRevLett.125.222003.

[21] R. Aaij et al. "Observation of the Decay $\Lambda_b^0 \to \Lambda_c^+ \tau^- \bar{\nu}_\tau$". In: *Physical Review Letters* 128.19 (May 2022). ISSN: 1079-7114. DOI: 10.1103/physrevlett.128.191803. URL: http://dx.doi.org/10.1103/PhysRevLett.128.191803.

[22] Minoru Tanaka and Ryoutaro Watanabe. "New physics in the weak interaction of $\bar{B} \to D^{(*)} \tau \bar{\nu}$". In: *Physical Review D* 87.3 (Feb. 2013). ISSN: 1550-2368. DOI: 10.1103/physrevd.87.034028. URL: http://dx.doi.org/10.1103/PhysRevD.87.034028.

[23] S. Hirose et al. "Measurement of the τ lepton polarization and $R(D^*)$ in the decay $\bar{B} \to D^* \tau^- \bar{\nu}_\tau$ with one-prong hadronic τ decays at Belle". In: *Physical Review D* 97.1 (Jan. 2018). ISSN: 2470-0029. DOI: 10.1103/physrevd.97.012004. URL: http://dx.doi.org/10.1103/PhysRevD.97.012004.

[24] Ashutosh Kumar Alok et al. "D^* polarization as a probe to discriminate new physics in $B \to D^* \tau \bar{\nu}$". In: *Physical Review D* 95.11 (June 2017). ISSN: 2470-0029. DOI: 10.1103/physrevd.95.115038. URL: http://dx.doi.org/10.1103/PhysRevD.95.115038.

[25] Belle Collaboration et al. *Measurement of the D^{*-} polarization in the decay $B^0 \to D^{*-} \tau^+ \nu_\tau$*. 2019. arXiv: 1903.03102 [hep-ex]. URL: https://arxiv.org/abs/1903.03102.

[26] A. G. Akeroyd and Chuan-Hung Chen. "Constraint on the branching ratio of $B_c \to \tau \bar{\nu}$ from LEP1 and consequences for $R(D^{(*)})$ anomaly". In: *Phys. Rev. D* 96.7 (2017), p. 075011. DOI: 10.1103/PhysRevD.96.075011. arXiv: 1708.04072 [hep-ph].

[27] Chao-Hsi Chang et al. "The lifetime of the B_c meson and some relevant problems". In: *Physical Review D* 64.1 (May 2001). ISSN: 1089-4918. DOI: 10.1103/physrevd.64.014003. URL: http://dx.doi.org/10.1103/PhysRevD.64.014003.

[28] Martin Beneke and Gerhard Buchalla. "The B_c meson lifetime". In: *Physical Review D* 53.9 (May 1996), pp. 4991–5000. ISSN: 1089-4918. DOI: 10.1103/physrevd.53.4991. URL: http://dx.doi.org/10.1103/PhysRevD.53.4991.

[29] R. L. Workman et al. "Review of Particle Physics". In: *PTEP* 2022 (2022), p. 083C01. DOI: 10.1093/ptep/ptac097.

[30] Albert M Sirunyan et al. "Search for charged Higgs bosons in the $H^{\pm} \to \tau^{\pm}\nu_{\tau}$ decay channel in proton-proton collisions at $\sqrt{s} = 13$ TeV". In: *JHEP* 07 (2019), p. 142. DOI: 10.1007/JHEP07(2019)142. arXiv: 1903.04560 [hep-ex].

[31] *Search for diphoton resonances in the 66 to 110 GeV mass range using 140 fb^{-1} of 13 TeV pp collisions collected with the ATLAS detector*. Tech. rep. All figures including auxiliary figures are available at https://atlas.web.cern.ch/Atlas/GROUPS/PHYSICS/CONFNOTES CONF-2023-035. Geneva: CERN, 2023. URL: https://cds.cern.ch/record/2862024.

[32] The Belle Collaboration et al. *Measurement of $\mathcal{R}(D)$ and $\mathcal{R}(D^*)$ with a semileptonic tagging method*. 2019. arXiv: 1904.08794 [hep-ex]. URL: https://arxiv.org/abs/1904.08794.

[33] Marat Freytsis, Zoltan Ligeti, and Joshua T. Ruderman. "Flavor models for $\bar{B} \to D^{(*)}\tau\bar{\nu}$". In: *Physical Review D* 92.5 (Sept. 2015). ISSN: 1550-2368. DOI: 10.1103/physrevd.92.054018. URL: http://dx.doi.org/10.1103/PhysRevD.92.054018.

[34] Abdelhak Djouadi. "The anatomy of electroweak symmetry breaking". In: *Physics Reports* 457.1–4 (Feb. 2008), pp. 1–216. ISSN: 0370-1573. DOI: 10.1016/j.physrep.2007.10.004. URL: http://dx.doi.org/10.1016/j.physrep.2007.10.004.

[35] Zhi-zhong Xing, He Zhang, and Shun Zhou. "Updated Values of Running Quark and Lepton Masses". In: *Phys. Rev. D* 77 (2008), p. 113016. DOI: 10.1103/PhysRevD.77.113016. arXiv: 0712.1419 [hep-ph].

[36] Jerome I Friedman and Henry W Kendall. "Deep inelastic electron scattering". In: *Annual Review of Nuclear Science* 22.1 (1972), pp. 203–254.

[37] A. D. Martin et al. "Uncertainties on α_S in global PDF analyses and implications for predicted hadronic cross sections". In: *The European Physical Journal C* 64.4 (Oct. 2009), pp. 653–680. ISSN: 1434-6052. DOI: 10.1140/epjc/s10052-009-1164-2. URL: http://dx.doi.org/10.1140/epjc/s10052-009-1164-2.

[38] M Spira et al. "Higgs Boson Production at the LHC". In: (Apr. 1995). arXiv: hep-ph/9504378 [hep-ph].

[39] "BSM Higgs production cross sections at $\sqrt{s} = 13\,\text{TeV}$ ". In: (2016). URL: https://twiki.cern.ch/twiki/bin/view/LHCPhysics/CERNYellowReportPageBSMAt13TeV.

[40] J. Alwall et al. "The automated computation of tree-level and next-to-leading order differential cross sections, and their matching to parton shower simulations". In: *JHEP* 07 (2014), p. 079. DOI: 10.1007/JHEP07(2014)079. arXiv: 1405.0301 [hep-ph].

[41] R. Frederix et al. "The automation of next-to-leading order electroweak calculations". In: *JHEP* 07 (2018). [Erratum: JHEP 11, 085 (2021)], p. 185. DOI: 10.1007/JHEP11(2021)085. arXiv: 1804.10017 [hep-ph].